Catalysis Today 155 (2010) 227–240

Contents lists available at ScienceDirect

Catalysis Today

journal homepage: www.elsevier.com/locate/cattod

Operando investigation of the catalytic behavior of Wells–Dawson heteropolycompounds in the oxidation of propene

E. Arendt, S. Ghislain, E.M. Gaigneaux *

Unité de catalyse et chimie des matériaux divisés, Université catholique de Louvain, Croix du Sud 2/17, 1348 Louvain-la-Neuve, Belgium

ARTICLE INFO

Article history:
Available online 18 January 2010

Keywords:
Wells–Dawson heteropolycompound
In situ characterization
Propene oxidation
Operando investigation

ABSTRACT

A complete characterization of the solid-state behavior of the Wells–Dawson heteropolycompounds in relevant conditions for a catalytic oxidation reaction in the gas phase was obtained by following the evolution of the Wells–Dawson salt under reducing and oxidizing model conditions by *in situ* X-ray diffraction analyses and *in situ* Raman spectroscopy. It was found that the oxido-reduction strength of the working condition is a tool to control the rearrangement of the Wells–Dawson compound into oxide species. Precisely, an oxidizing feed was shown to stabilize the Wells–Dawson compound, i.e. delay the irreversible transformation of the structure to a mixture of oxides, and thus may be used to modulate the catalytic behavior of the catalyst. Looking for the influence of the oxido-reduction atmosphere, an operando setup combining Raman spectroscopy with online analysis of gaseous products of the catalytic propene oxidation was then used to gain further information on the solid-state behavior of Wells–Dawson heteropolycompounds at work. Along a reaction temperature profile, a peak of propene conversion could be obtained. This was hypothesized to be due to the *in situ* formation of a propene-containing bronze Mo oxide looking phase. The formation of such phase seems to be facilitated when a more reductive atmosphere is applied on the Wells–Dawson during the reaction.

1. Introduction

Heteropolycompounds are finding increasing use as catalysts due to their tunable both redox and acid–base properties [1–6]. An interesting aspect is that heteropolycompound solids appear as inherently unstable materials during operation as gas phase oxidation catalysts [7]. A consistent picture was already elaborated of the solid-state rearrangement occurring during response of heteropolycompounds to the thermal and chemical conditions of selective oxidation catalysis [7]. A benefit of this behavior could be that by applying an adequate treatment, heteropolycompounds could act as precursors to the desired more active species which truly make a given catalytic job.

Previous research performed indeed confirmed this hypothesis, showing that when catalyzing the reaction of 2-butanol in presence of oxygen, Wells–Dawson heteropolycompound were forced to *in situ* undergo a continuous structural rearrangement in the course of the process and presented at an intermediate state of their rearrangement, an enhanced selectivity in methyl-ethyl-ketone (MEK) as compared to selectivities to less desired COx and butenes [8]. From then, our research was directed to the identification of a tool to control the reorganisation of the Wells–Dawson heteropolycompounds, and to stabilize the more active intermediate species. The possibility to succeed such stabilization via the adjustment of the oxido-reduction strength of the gas phase was investigated [9]. The reaction of 2-butanol in the presence of O_2 was therefore conducted with O_2:2-butanol ratios varied in the range 1–10. The best stability of the selectivity towards MEK was obtained at a ratio of 5. Characterization suggested that the catalyst working under these conditions was undergoing structural modifications with time on stream while the catalytic performances remain constant. The catalyst at work never really had the perfect structure of a heteropolycompound, namely the tested samples presented features of the Wells–Dawson or/and molybdenum oxide phases together with crystalline and molecular features of a Keggin anion [9]. This work evoked that the highest performances were obtained on a 'living' catalyst, likely with a wobbly structure, that was formed *in situ*.

Our previous works also indirectly demonstrated that a tool to control the reorganisation of the Wells–Dawson heteropolycompound, and hopefully to stabilize this intermediate living species, is to place the catalyst in gas conditions with an oxido-reduction strength properly adjusted [8,9]. The nature of the more active intermediate and the reasons why it is indeed more active are not elucidated at this stage.

Determining and understanding structure/composition-activity/selectivity relationships for operating $(NH_4)_6P_2Mo_{18}O_{62}$ heteropolycompound are thus of crucial interest. In others words, a key to

* Corresponding author. Fax: +32 10 47 36 49.
E-mail address: eric.gaigneaux@uclouvain.be (E.M. Gaigneaux).

0920-5861/$ – see front matter © 2009 Elsevier B.V. All rights reserved.
doi:10.1016/j.cattod.2009.11.020

progress is now to track the physico-chemical processes taking place in the Wells–Dawson catalyst in real time and under operating conditions in order to study the relationships between thermal treatment under red/ox conditions and the structural/molecular features of the Wells–Dawson catalyst. Thus, to obtain a more complete characterization of the solid-state behavior of the Wells–Dawson salt in relevant conditions for a catalytic oxidation reaction in the gas phase, the evolution of the Wells–Dawson salt $(NH_4)_6P_2Mo_{18}O_{62}$ under reducing and oxidizing model conditions was first followed by *in situ* X-ray diffraction analyses and *in situ* Raman spectroscopy. Then, an *operando* setup combining Raman spectroscopy with online analysis of gaseous products of the catalytic propene oxidation was used to gain further information on the solid-state behavior of Wells–Dawson salts. For purpose of comparison, Mo trioxide and Keggin catalysts were tested in the catalytic propene oxidation.

2. Experimental

2.1. Synthesis of the ammonium phospho-molybdic Dawson-type salt $(NH_4)_6P_2Mo_{18}O_{62}$

The Dawson salt $(NH_4)_6P_2Mo_{18}O_{62}$ was synthesized according to Wu [10]. A mixture of 85.12 g of Na_2MoO_4 (Aldrich 98+%), 15 mL of concentrated H_3PO_4 (Janssen Chimica 85%) and 80 mL of concentrated HCl (Sigma–Aldrich 37%) in 450 mL of distilled water was kept boiling for 8 h. The mixture was then cooled to room temperature and 100 g of NH_4Cl (Sigma–Aldrich 99.5+%) were added. The precipitation of a solid was observed immediately after the addition of ammonium chloride. The solid was filtered through a Büchner funnel and redissolved in an equal weight of distilled water. This solution was filtered through hardened paper (Whatman no. 2) to separate eventual undissolved impurities. To the perfectly clear solution, solid NH_4Cl was added, to make a 20 wt.% solution without stirring. After standing for 4–8 h the crystals were transferred into a Büchner funnel, sucked as dry as possible and redissolved in the minimum amount of distilled water. The resulting solution was evaporated in a rotary evaporator (40 °C) under reduced pressure until crystals began to form. The precursor and the supernatant solution were kept at 5 ° C overnight. Finally, the salt was filtered, washed with anhydrous diethyl ether (10 mL Merck 99.7+%) and dried at room temperature under vacuum.

2.2. Synthesis of the phospho-molybdic Keggin acid $H_3PMo_{12}O_{40}$

The Keggin heteropolyacid was obtained through the 'etherate method' [10]. 45.55 g of Na_2MoO_4 (Aldrich 98+%) were dissolved in 100 mL of distilled water. 5 mL of concentrated H_3PO_4 (Janssen Chimica 85%) and 50 mL of concentrated HCl (Sigma–Aldrich 37%) were added. This acidified aqueous solution of the heteropolyanion was transferred to a 1 L separatory dropping funnel and mixed together with diethyl ether (75 mL Merck 99.7+%). After standing for 10–15 min, three layers were formed: an upper ether layer, an intermediate aqueous layer and a heavy oily layer. The dropping funnel was cooled under the tap water and the lowest layer was transferred to another dropping funnel with 50 mL of distilled water and shaken. Then, 50 mL of concentrated HCl and 75 mL of diethyl ether were added and the resulting solution was shaken again. After cooling, the lowest layer was again transferred to another dropping funnel and washed once more. Finally, the ethereal solution, which was perfectly clear, was transferred to a beaker containing 12.5 mL of distilled water and a few drops of concentrated HNO_3 (Merck 65%) were added. The resulting solution was evaporated on a water bath with occasional stirring until crystals began to form on the surface. The crystals were allowed to cool down to room temperature and were filtered through a Büchner funnel. Charaterization data of this sample are descibed in [8].

2.3. Synthesis of the ammonium phospho-molybdic Keggin-type salt $(NH_4)_3PMo_{12}O_{40}$

The Keggin $(NH_4)_3PMo_{12}O_{40}$ was prepared according to [11]. 15.44 g of $H_3PMo_{12}O_{40}$ prepared as described above (Section 2.2), were dissolved in 30 mL of distilled water. A solution containing 12.08 g of NH_4Cl (Sigma–Aldrich 99.5+%) in 30 mL of distilled water was quickly added. The resulting suspension was filtered through a Büchner funnel and the recovered solid was washed twice with distilled water. Finally, the salt was dried on a Büchner funnel [11]. Characterization data of the ammonium phospho-molybdic Keggin sample are given in [8].

2.4. Synthesis of the Mo trioxide

The Mo trioxide constituted of crystals with an isotropic morphology was prepared by decomposing $(NH_4)_6Mo_7O_{24}.7H_2O$ at 773 K in air during 20 h. Preparation details and characterization of this sample are described in [12] (in [12], the MoO_3 sample is denoted MoO_3-III).

2.5. Catalyst characterizations

The identity and purity of the ammonium phospho-molybdic Dawson salt $(NH_4)_6P_2Mo_{18}O_{62}$ sample were checked using X-ray diffraction (XRD), FTIR, Raman spectroscopy, X-ray photoelectron spectroscopy (XPS) and elementary analyses.

X-ray diffraction (XRD) patterns were recorded on a Siemens D5000 diffractometer using the Kα radiation of Cu ($\lambda = 1.5418$ Å). The 2θ range was scanned between 5° and 80° at a rate of 0.01° s^{-1}. The identification of the phases was achieved by using the ICDD-JCPDS database.

Fourier transformed infra red spectra (FTIR) were recorded in the transmission mode using a IFS55 Equinox spectrometer (Brücker) equipped with a DTGS detector. The spectra were obtained by recording 100 scans between 370 and 4400 cm^{-1} with a resolution of 4 cm^{-1}. Wafers were prepared after diluting the sample in KBr (Janssens Chimica 99+%) by a weight factor of 100.

Fourier transformed Raman spectroscopy was performed with a Brücker RFS100/S, equipped with a Nd-YAG ($\lambda = 1064$ nm) laser. The spectra were recorded in the Raman shift range between 200 and 2000 cm^{-1}. The spectral resolution was 4 cm^{-1}, and the spectra acquisition consisted of 32 accumulations for each sample.

X-ray photoelectron spectroscopy (XPS) analysis was performed on a Kratos Axis Ultra spectrometer (Kratos Analytical, Manchester, UK) equipped with a monochromatized aluminium X-ray source (powered at 10 mA and 15 kV) and an eight channeltrons detector. The pressure in the analysis chamber was approximately 10^{-6} Pa. The pass energy was set at 160 eV for the wide scan and 40 eV for narrow scans. In the latter conditions, the full width at half maximum (FWHM) of the Ag 3d5/2 peak of a standard silver sample was about 0.9 eV. Charge stabilization was achieved by using the Kratos Axis device. The following sequence of spectra was recorded: survey spectrum, C 1s, O 1s, Cl 2p, P 2p, Mo 3d, N 1s, Na 1s and C 1s again to check for charge stability as a function of time and the absence of degradation of the sample during the analysis. The C-(C,H) component of the C 1s peak of carbon was fixed to 284.8 eV to set the binding energy scale. The intensity ratio I (Cl 2p3/2)/I (Cl 2p1/2) was fixed at 2, with an energy difference of 1.6 eV [13]. The intensity ratio I (P 2p3/2)/I (P 2p1/2) was fixed at 2, with an energy difference of 0.84 eV [13]. Decomposition of the Mo 3d doublets was done by fixing as constraints an energy difference of 3.13 eV and an area ratio of 2/3

between the Mo 3d3/2 and the Mo 3d5/2 bands [13]. As another constraint, the FWHM's of the two contributions of a doublet were kept identical during the whole decomposition process. Peaks were considered to be combinations of Gaussian and Lorentzian functions in a 70/30 ratio working with a linear baseline. For the quantification of the elements, sensibility factors provided by the manufacturer were used. Data treatment was performed with the CasaXPS program (Casa Software Ltd., UK).

The elemental analysis of Mo and P in the catalyst was performed by atomic absorption spectrophotometry using inductively coupled plasma optical emission spectroscopy (IRIS Advantage de Thermo Jarrel Ash).

2.6. In situ characterizations

Thermodiffractometry analyses were performed on the Siemens D5000 diffractometer apparatus equipped with a high temperature chamber HTK10 from Anton Paar. In this device, the sample were mounted on a holder made of a Pt plate electrically borned. The sample heating was done by adjusting the current through the plate via a specific controller, and a thermocouple touching the plate. A direct heating was thus achieved allowing a high temperature stability and accurate ramping of temperature (heating and cooling) without over- or downshooting. The chamber was closed by a flask presenting a X-ray transparent window made of Kapton and connections allowing inlet and outlet of gases, eventually flowing through the chamber, or vacuum. The samples were analysed in the range 5–45° with increment of 0.02° per 1s. XRD patterns were measured stepwise every 50 °C in the temperature range 100–400 °C. In each case, a first and a last X-ray diffraction patterns were recorded at 30 °C. The different temperatures were reached at a rate of 0.2 °C/s and a delay of 60 min was respected before the collection of the pattern was started expected for the first one at 30 °C which was recorded after a delay of 10 s. The experiments were made respectively under flowing O_2 (Praxair 4.5)/He (Praxair 4.6) (1:2), He (Praxair 4.6) and H_2/He (Praxair) (10:90) (60 mL/min). The presence of the Pt plate explains that all X-ray patterns contains the diffraction line of Pt (ICDD-JDPDS 04-0802, $2\theta = 39.76°$).

Raman *in situ* spectra were recorded with a Kaiser RXN spectrometer (diode-pumped frequency doubled Nd-YAG laser with 532 nm wavelength, power ca. 50 mW, Mk II filtered probehead with 5.5 in. noncontact objective, spot-size ca. 100 μm). The powdered catalysts were introduced into a quartz reactor with two optical windows. The reactor was positioned in the center of a hollow stainless steel cylinder heated by four cartridge heaters inserted around the central hole. A hole was drilled horizontally in the cylinder so that the long focal objective could be focused on the catalyst in the reactor so as to bring the incident laser, and collected the Raman signal, to and from the sample. The reactor was connected to a gas factory to allow a flowing gas inlet of different compositions. This setup was inspired from that described in [14,15]. In the experiments, the investigated sample was heated from 25 to 400 °C (stepwise 25 °C, staying time of 60 min) under O_2 (Praxair 4.5)/He (Praxair 4.6) (1:3) and He (Praxair 4.6) (30 mL/min). The Raman spectra were recorded every 4 min in the spectral range from 100 to 4350 cm^{-1} Raman shift with a resolution of 5 cm^{-1}. A correct calibration of the Raman spectrometer was assumed by no deviation of the Raman fingerprint of well crystallized MoO_3 (preparation details and characterization of this sample are described in [12] (in [12], the MoO_3 sample is denoted MoO_3-III)) regularly measured. The signal attributed to the O= Mo= O bond always falls at 995 cm^{-1} as reported in [7]. For all *in situ* Raman experiments, the reader should pay attention that the intensity of the line inside a figure cannot be compared directly due to experimental reality. Indeed, the conditions for recording are probably changing during the heating in terms of the occurrence of some defocusing of the laser beam on the solid.

2.7. Catalytic tests—operando procedure

Catalytic tests were performed operando in the Raman setup described above, additionally interfaced with an on line system for the analysis of the gaseous products at the outlet of the quartz reactor. Powdered catalyst was introduced into the quartz reactor and covered by glass beads. No conversion of C_3H_6 is observed over the glass beads during a reaction test run between 250 and 500 °C (stepwise every 50 °C with a staying time of 120 min) with a gaseous mixture of 20%O_2, 10%C_3H_6 and 70%He (total flow set at 30 mL/min). The reaction temperature was measured with a thermocouple positioned inside the catalytic bed. Gaseous products were analysed every 2 min 30 s, by an Interscience compact gas chromatograph equipped a Rtx-1, 1.5 μ column (15 m × 0.32 mm) followed by a FID, a Poraplot Q (2 m × 0.32 mm) and a Molsieve 5 Å column (5 m × 0.32 mm) followed by a TCD and two Poraplot Q columns (2 m and 8 m × 0.32 mm) followed by a second TCD. Spectroscopic analysis of the catalysts inside the reactor was carried out during the catalytic tests. Raman spectra were recorded every 4 min in the spectral range from 100 to 4350 cm^{-1} Raman shift with a resolution of 5 cm^{-1}. Three tests were done to investigate the behavior of the $(NH_4)_6P_2Mo_{18}O_{62}$ sample under real catalytic conditions. In order to tune the ratio O_2:C_3H_6 in the reaction feed, the flow of propene was always of 10% with correspondingly the flow He and O_2 adjusted to keep the total gas flow constant set a 30 mL/min. O_2:C_3H_6 ratios investigated were 2, 1 and 0.5. Thus, at each test, a different gaseous mixture was fed into the reactor, namely (i) a gaseous mixture of 70 vol.% He, 10 vol.% C_3H_6 and 20 vol.% O_2 ($O_2/C_3H_6 = 2$), (ii) a gaseous mixture of 80 vol.% He, 10 vol.% C_3H_6 and 10 vol.% O_2 ($O_2/C_3H_6 = 1$), and (iii) a gaseous mixture of 75 vol.% He, 10 vol.% C_3H_6 and 5 vol.% O_2 ($O_2/C_3H_6 = 0.5$). For each test, the same temperature program was used. The reaction test was run between 250 and 450 °C, stepwise every 50 °C with a staying time of 2 h expected for the last step at 450 °C which has a staying time of 8 h. For these steps, the temperature rate was always of 1 °C/min. To avoid overshooting of temperature, the reactor was first heated up to 100 °C (temperature rate of 10 °C/min, staying time of 1 min) and secondly to 200 °C (temperature rate of 10 °C/min, staying time of 1 min) before heated up to 250 °C. At the end of the process, the reactor was cooled down under the same gaseous feed. Acrolein, acetaldehyde, CO and CO_2 are the main products detected. Other compounds (i.e. acetic acid, propene oxide, acetone and acid acrylic) are also detected but only in traces and were thus not considered. Catalytic activity is here reported in terms of conversion of C_3H_6 (number of moles of propene converted per 100 moles of propene introduced), selectivities (SC_3H_4O, SCH_3CHO, SCO/CO_2 number of moles of acrolein, acetaldehyde, CO and CO_2 produced per 100 moles of propene converted; in the case of CO/CO_2 a factor 3 was taken into account) and carbon balances.

3. Results

3.1. Identity and purity of $(NH_4)_6P_2Mo_{18}O_{62}$ sample

Fig. 1 presents the X-ray diffraction pattern of the $(NH_4)_6P_2Mo_{18}O_{62}$ sample. This pattern equally agrees both with those likely incomplete patterns reported in the literature namely $(NH_4)_6P_2Mo_{18}O_{62} \cdot 12H_2O$solid [16] and $(NH_4)_6H_6(P_2O_2(Mo_2O_7)_9)\cdot 7H_2O$ compounds (ICDD-JDPDS 04-0443). However, the X-ray pattern also contains the diffraction lines of NH_4Cl (ICDD-JDPDS 01-0674) and of $(NH_4)_3PO_4(MoO_3)_{12} \cdot 4H_2O$ (ICDD-JDPDS 09-0412).

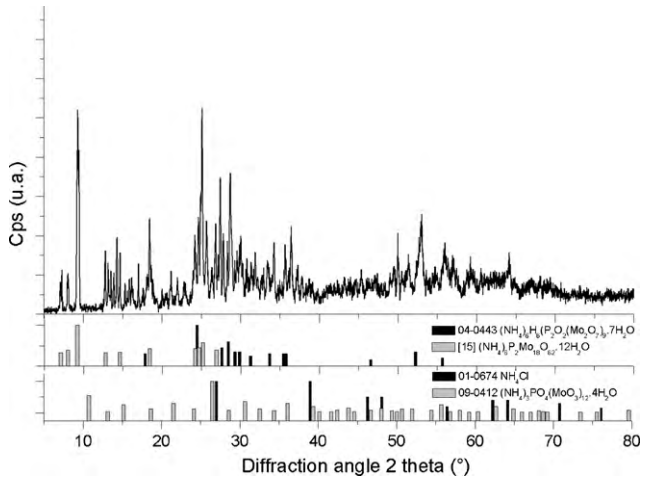

Fig. 1. X-ray diffraction of the fresh $(NH_4)_6P_2Mo_{18}O_{62}$ sample. Peak positions for the reference $(NH_4)_6P_2Mo_{18}O_{62} \cdot 12H_2O$ [16], $(NH_4)_6H_6(P_2O_2(Mo_2O_7)_9) \cdot 7H_2O$ (ICDD-JCPDS 04-0443), NH_4Cl (ICDD-JCPDS 01-0674), $(NH_4)_3PO_4(MoO_3)_{12} \cdot 4H_2O$ (ICDD-JCPDS 09-0412) phases are also given for comparison.

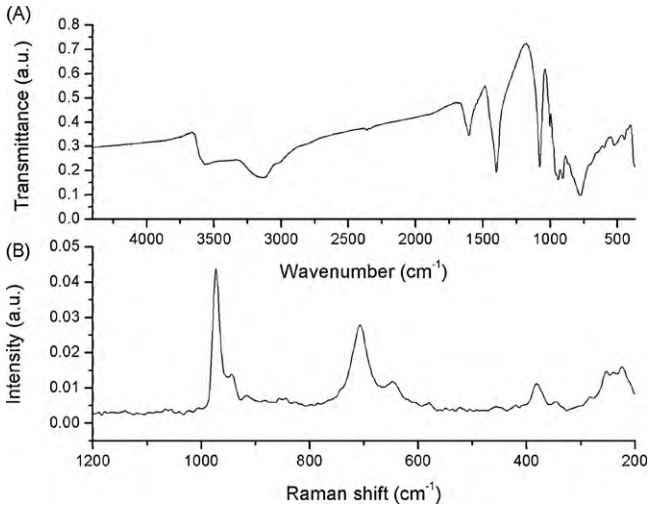

Fig. 2. (A) Infrared spectrum and (B) Raman spectrum of the fresh $(NH_4)_6P_2Mo_{18}O_{62}$ sample.

Both compounds represent residues of the synthesis. Nevertheless, the intensity of these lines are weak and it thus seems that the sample contains mainly the desired Wells–Dawson heteropoly-compound.

In addition, the sample $(NH_4)_6P_2Mo_{18}O_{62}$ presents infrared vibrations at 1076 and 906 cm^{-1}, and at 940 and 777 cm^{-1} which are respectively characteristic for the central phosphorous species, and Mo–O species in phospho-molybdic Wells–Dawson structure as reported in the literature [16,17] (Fig. 2(A)). Our salt also exhibits the infrared signal of the NH_4^+ species at 1400 cm^{-1}[16,17]. The Raman spectrum (Fig. 2(B)) possesses two major signals at 973 and 707 cm^{-1}, indeed characterizing the Dawson heteropoly-oxoanion [16,17]. The signals in the 830–1000 cm^{-1} range are attributed to the stretching modes of the terminal Mo = O bonds, and the signals at 648 and 703 cm^{-1} might be assigned to the Mo–O–Mo stretching [17].

The observations that the infrared and Raman spectra possess signals of Dawson heteropolycompounds and that the X-ray diffraction mainly reveals the lines of a solid built with Wells–Dawson anions evidence the identity of the synthesized materials. Furthermore, elemental analysis confirms the purity of the sample as the Mo/P atomic ratio found by ICP is 9.0 and as the surface Mo/P atomic ratio found by XPS is 7.4. In the same nature of ideas, the XPS experimental N/P atomic ratio is equal to the theoretical one (3). A weak chloride XPS contribution, corresponding to a surface %Cl of 0.25 (2p3/2 contribution at a binding energy of 198.3 eV) is observed. The $(NH_4)_6P_2Mo_{18}O_{62}$ sample exhibits mainly a doublet Mo 3d with the 3d5/2 contribution at a binding energy of 233.3 eV characteristic of the most oxidized state of Mo species (namely, Mo^{6+}) [18]. Besides the P 2p peak for this sample was characteristic of P in the 5+ oxidation state (2p3/2 contribution at binding energy of 133.7 eV).

3.2. In situ X-ray diffraction

Fig. 3 presents the XRD patterns measured stepwise every 50 ° C in the temperature range 100–400 ° C under (A)) O_2/He, (B) He

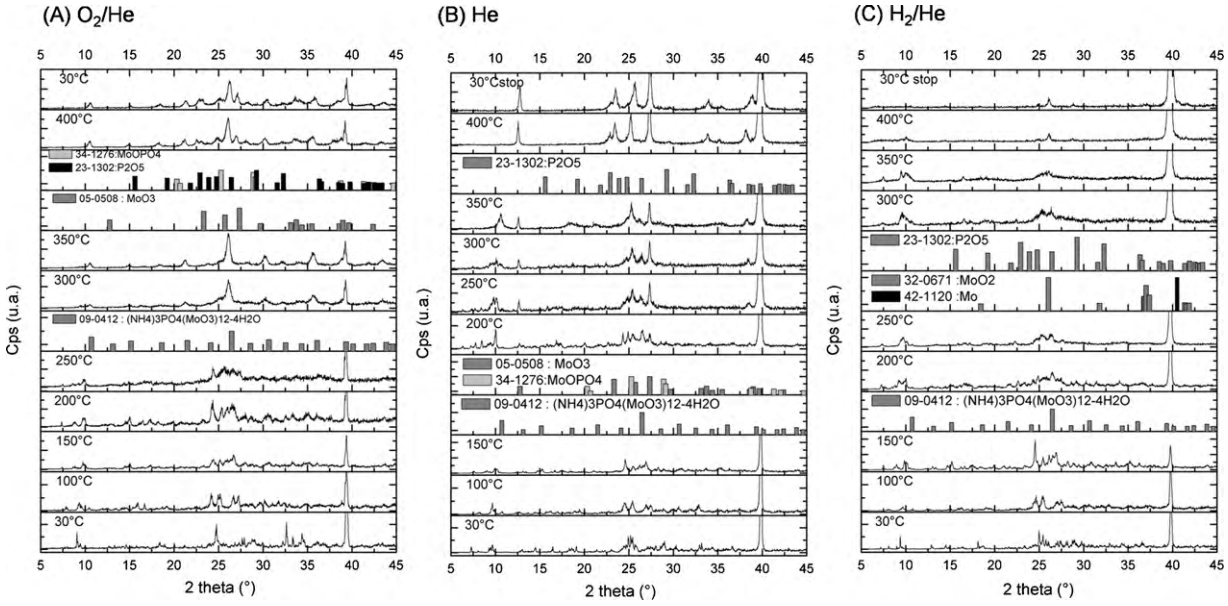

Fig. 3. XRD patterns measured stepwise every 50 ° C in the temperature range 100–400 ° C under (A) O_2/He, (B) He and (C) H_2/He. Due to experimental reality, absolute intensities are not significant, only relative intensities can be discussed.

Table 1
In situ X-ray diffraction as a function of the gaseous conditions. WD means Wells–Dawson $(NH_4)_6P_2Mo_{18}O_{62}$, K = Keggin $(NH_4)_3PO_4(MoO_3)_{12}\cdot 4H_2O$ ICDD-JCPDS 09-0412,Mo = Mo ICDD-JCPDC 42-1120, MO3 = MoO_3 ICDD-JCPDS 05-0508, MO2 = MoO_2 ICDD-JCPDC 32-0671, PO = P_2O_5 ICDD-JDPDC 23-1302, MoOP = $MoOPO_4$ ICDD-JDPDC 34-1276.

Feeds	100 °C	150 °C	200 °C	250 °C	300 °C	350 °C	400 °C
O_2/Hec	WD			WD → K	K		K → MO3 + MoOP + PO
He	WD		WD → K + MO3 + MoOP			K → MO3 + MoOP	MO3 + MoOP + PO
H_2/He	WD		WD → K		K → MO2 + Mo	MO2 + Mo + PO	

and (C) H_2/He (10:90). The results are summarized in Table 1. Firstly, it can be observed that an oxidizing atmosphere stabilizes the Wells–Dawson structure. Under an oxidizing feed, the crystalline structure of the Wells–Dawson sample remains intact up to 200 °C, while the Wells–Dawson sample tends to turn progressively to a Keggin sample at a lower temperature under both inert (He) and reductive (H_2/He) atmosphere. Indeed, under an oxidizing feed, the crystalline features of Keggin anion appear at 250 ° C ($2\theta = 26.5°$, which is the major diffraction line of the reference $(NH_4)_3PO_4(MoO_3)_{12}$ (ICDD-JCPDS 09-0412), and this structure is clearly observed on the X-ray pattern measured at 300 °C. Under reducing and inert conditions, typical diffraction lines of the Dawson anions are vanished at a lower temperature than under oxidizing feed. Fig. 3(B) shows the evolution of the crystalline feature of the $(NH_4)_6P_2Mo_{18}O_{62}$ sample under He at different temperatures. It can be observed that at 200 °C, the XRD pattern already contains the diffraction lines of Keggin anion (ICDD-JCPDS 09-0412, $2\theta = 26.5°$), MoO_3(ICDD-JCPDS 05-0508, $2\theta = 12.7$ and 27.3°), $MoOPO_4$(ICDD-JCPDS 34-1276, $2\theta = 25.3°$) while diffraction lines of Wells–Dawson anion, still present at 200 ° C (diffraction lines at approximatively $2\theta = 24°$) are vanished at 250 °C. At 200 ° C under reductive feed, for instance H_2/He (10:90) (Fig. 3(C)), the parent diffraction line of Keggin structure $(NH_4)_3PO_4(MoO_3)_{12}\cdot 4H_2O$ (ICDD-JCPDS 09-0412, $2\theta = 26.5°$) appears while the typical signs of a Wells–Dawson structure already progressively vanish (2θ between 24–25°).

Secondly, at a higher temperature, it can be noted that the crystalline structures of oxides species appear at higher temperature under oxidizing feed than under the other conditions. So, the reorganisation of the Keggin sample into oxide species is not facilitated by the presence of oxygen. *In situ* XRD results concerning the sample treated under O_2:He (Fig. 3(A)) show that features of Keggin anion remain up to 400 °C. In Fig. 3(A), a peak typical of MoO_3 phase (ICDD-JDPDC 05-0508 $2\theta = 27.3°$) appears at 400 ° C together with diffraction lines of $MoOPO_4$ (ICDD-JDPDC 34-1276, $2\theta = 25.3°$) and P_2O_5 (ICDD-JDPDC 23-1302, $2\theta = 22.9$ and 24.8°). On the other hand, as far as inert condition is concerned (Fig. 3(B)), the sample never acquires a perfect Keggin structure but always appears as a mixture of different phases, among which the Keggin phase. Indeed, the major diffraction line of $(NH_4)_3PO_4(MoO_3)_{12}\cdot 4H_2O$ structure appears at 200 ° C (ICDD-JCPDS 09-0412, $2\theta = 26.5°$) together with lines typical of MoO_3, $MoOPO_4$. At 300 °C, a second peak typical of Keggin anion is discernable ($2\theta = 10.7°$). It can be noticed that this peak appears (its intensity increases as seen on the pattern at 350 °C) while the intensity of the principal peak of the Keggin phase at $2\theta = 26.7$ diminishes. At 400 °C, the sample presents a mixture of MoO_3 (ICDD-JDPDC 05-0508, $2\theta = 23.3, 25.7$ and 27.3°), $MoOPO_4$ (ICDD-JDPDC 34-1276, $2\theta = 25.3°$) and P_2O_5 (ICDD-JDPDC 23-1302, $2\theta = 22.9°$) phases. As observed under He, the sample never acquires a perfect Keggin structure under a reductive atmosphere. Under H_2/He feed (Fig. 3(C)), typical feature of the Keggin structure appear at 200 ° C (ICDD-JCPDS 09-0412, $2\theta = 26.5°$) while peaks of the Dawson anion are already mostly vanished. At 300 °C, the crystalline structure is modified and at 350 °C, the sample presents the X-ray diffraction lines of MoO_2 phase (ICDD-JCPDC 32-0671, 2 $\theta = 26.0°$), Mo (ICDD-JCPDC 42-1120 $2\theta = 40.5°$) and P_2O_5 (ICDD-JDPDC 23-1302, $2\theta = 24.8°$) phases.

3.3. *In situ* Raman

In this section, the Raman spectra are mainly presented as contour graphs (Figs. 4(A) and 5(A)). Contour graphs are surface graphs of *xyz* data, plotted in 2D space. In this case, the *x* data are the Raman shift (cm^{-1}); the *y* data are the time (min) and the *z* data are the intensity of the Raman spectra (u.a.), ranges of *z* values are distinguished by different gray levels. In addition, a second layer is plotted on these contour graphs, namely the temperature profile (°C) as a function of time (min). Moreover, to improve the analysis of Raman spectra, selected Raman, at the end of the different plateaux, are reported in Figs. 4(B) and 5(B). Table 2 summarizes the Raman signals of the Wells–Dawson ($(NH_4)_6P_2Mo_{18}O_{62}$ and $H_6P_2Mo_{18}O_{62}$), Keggin ($(NH_4)_3PMo_{12}O_{40}$ and $H_3PMo_{12}O_{40}$) heteropolycompounds and MoO_3 based on spectroscopic studies reported in the literature [16,17,19–22,7]. Fig. 4(A) presents the contour graph obtained during the thermal treatment of the $(NH_4)_6P_2Mo_{18}O_{62}$ sample under O_2/He, selected Raman spectra for this experiment are presented in Fig. 4(B). It appears that the structure of the Wells–Dawson anion remains intact up to 150 ° C (the main characteristic Raman bands of the Wells–Dawson sample are still observed (380, 653, 708 and 970 cm^{-1})), while at higher temperature, structural changes and rearrangements are observed. Indeed, at 175 °C, the structure starts to change as the intensities of the Raman bands at 380, 653 and 708 cm^{-1} diminish and, between 200 and 225 °C, the Wells–Dawson compound rearranges with the formation of a phase containing the Keggin unit (Raman bands at 603, 871, 967 and 980 cm^{-1}). The Keggin structure is preserved at higher temperature (Raman bands at 603, 870, 965 and 980 cm^{-1} characterizing the $(NH_4)_3PMo_{12}O_{40}$ heteropolycompound and Raman bands at 965, 980 and 990 cm^{-1} characterizing the $H_3PMo_{12}O_{40}$ heteropolycompound). It can be observed that the Raman band at 817 cm^{-1} (sign of MoO_3) appears at 250 ° C and its intensity increases as a function of the temperature. The appearance of MoO_3 is confirmed by the Raman bands at 284 and 990 cm^{-1}. Above 375 °C, no further signs of a Keggin structure are observed.

The contour graph and the selected Raman spectra obtained during the thermal treatment of the $(NH_4)_6P_2Mo_{18}O_{62}$ sample under He are represented in Fig. 5(A) and (B), respectively. It appears that the main characteristic Raman bands of the Wells–Dawson sample are vanished at a lower temperature under an He(Fig. 5(A)) compared to the oxidizing condition (Fig. 4(A)). Indeed, at 125 °C, a decrease of the Raman bands'intensities at 380, 653 and 780 cm^{-1} is observed. At this temperature, the sample rearranges with the formation of the Keggin phase (Raman bands at 977, 968 and 871 cm^{-1}). No further interpretation of the contour graphs can be made above 250 °C.

With these *in situ* Raman investigations, X-ray diffraction analyses are confirmed as it was found that an oxidizing feed stabilizes Wells–Dawson heteropolycompounds catalysts compared to other inert or reducing atmospheres.

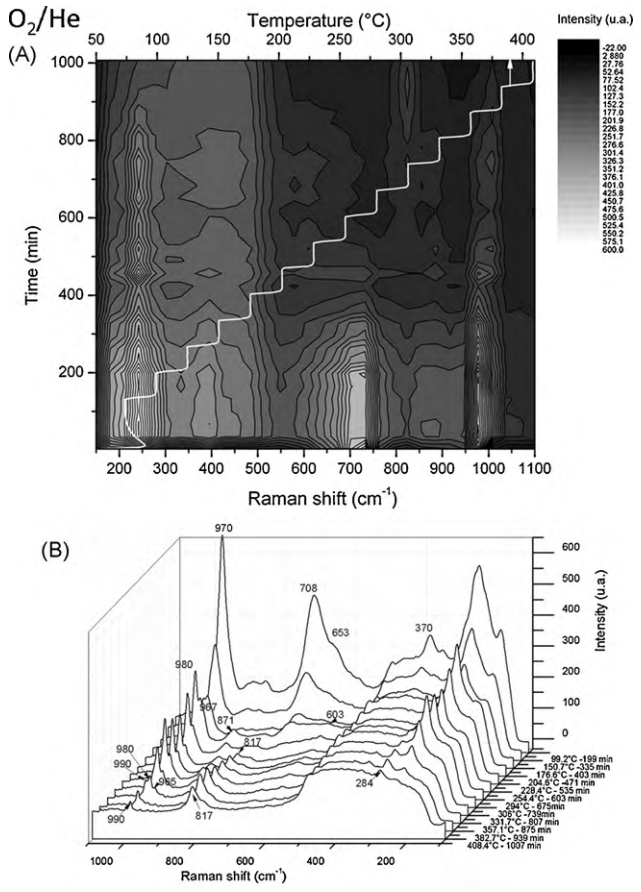

Fig. 4. Raman spectra recorded every 4 min during the thermal treatment of the $(NH_4)_6P_2Mo_{18}O_{62}$ sample from 25 to 400 ° C (stepwise 25 °C, staying time of 60 min) under O_2/He (1:3): (A) contour graphs and (B) selected Raman spectra.

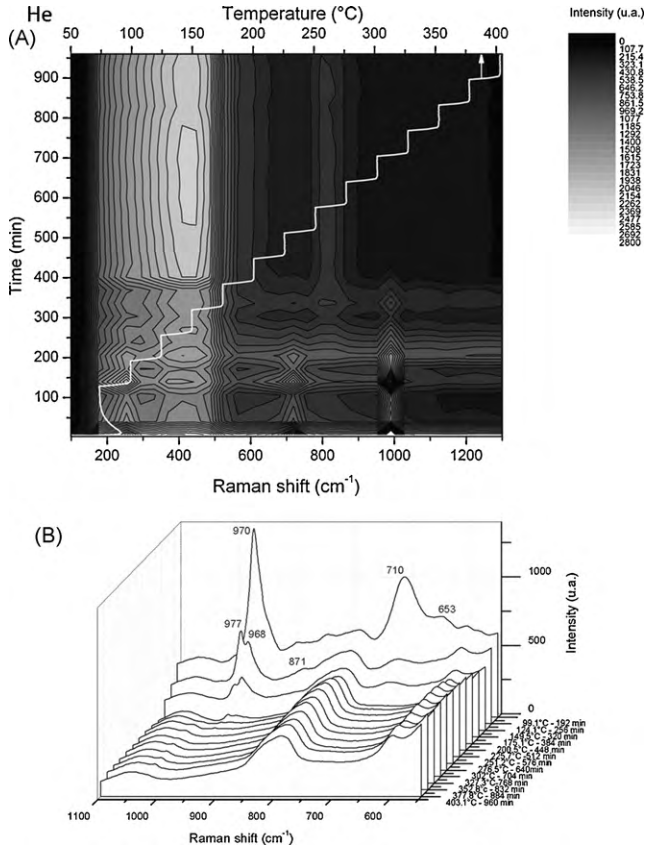

Fig. 5. Raman spectra recorded every 4 min during the thermal treatment of the $(NH_4)_6P_2Mo_{18}O_{62}$ sample from 25 to 400 ° C (stepwise 25 °C, staying time of 60 min) under He (30 ml min^{-1}). (A) Contour graphs and (B) selected Raman spectra (data below 600 cm^{-1} were not shown).

3.4. Operando results

The $(NH_4)_6P_2Mo_{18}O_{62}$ sample has been tested in the oxidation of propene under three different gaseous atmospheres: O_2/C_3H_6 ratio of 2, 1 and 0.5. Catalytic results obtained are reported in Figs. 6, 14 and 16, respectively. The conversion and the selectivities towards acrolein (SC_3H_4O), acetaldehyde (SCH_3CHO), CO and CO_2 (SCO/CO_2) are displayed in Figs. 6(A), 14(A) and 16(A) as a function of time. On these graphs, the temperature of the oven and the temperature measured with a thermocouple inside the catalytic bed are also reported. In Figs. 6, 14(B) and 16(B), the carbon balance is reported as a function of time on stream. During all the tests, the Raman spectra were measured stepwise every 4 min. In all cases, the Raman spectra of starting catalysts possess signals of Dawson heteropolycompounds as reported in Fig. 2. Selected Raman spectra are reported on Figs. 7, 15 and 17. For each test, Raman spectra at the beginning and at the end of the different plateaux (250, 300, 350, 400, 450 °C) were selected. For the last one (450 °C), more numerous Raman spectra were selected.

The results obtained for the first test (O_2/C_3H_6 ratio of 2) are summarized in Fig. 6. In the first part, below 350 °C, the catalyst exhibits a very weak catalytic activity ($\leq$ 5% of propene conversion). The second part of the graph, between 350 and 400 °C, reveals an increase of performances. The conversion curve shows an increasing trend up to 7% of propene conversion as a function of the increase of the temperature from 350 up to 400 °C. This increase is followed by a decreasing trend and finally, during the stabilization at 400 °C, the conversion reaches a stable level at $\propto$ 5%. During this step, the selectivities follow the same tendency (an increasing trend followed by a decrease and a plateau), and SCH_3CHO (40%) is higher than SC_3H_4O. The last part of the graph, between 400 and 450 °C, reveals two things. Firstly, the conversion increases with the temperature and reaches 20%. This increase is followed by a decreasing trend and a stabilization at 10%. Secondly, the selectivity to acetaldehyde decreases, that to CO/CO_2 increases and the selectivity towards acrolein product remains at a relatively stable level (20%). Raman spectra selected for this first catalytic test (O_2/C_3H_6 ratio of 2) are displayed on Fig. 7. It can be observed that during the plateau at 250 °C, the molecular structure of the catalyst is modified. Indeed, at the beginning of the plateau, the Raman spectrum possesses two major signals at 965 and 702 cm^{-1} while, the Raman spectrum at the end of this plateau, possesses a

Table 2
Summary of the major Raman signals of the $(NH_4)_6P_2Mo_{18}O_{62}$, $H_6P_2Mo_{18}O_{62}$, $(NH_4)_3PMo_{12}O_{40}$, $H_3PMo_{12}O_{40}$ and MoO_3 samples.

Sample	Major Raman signals (cm^{-1})					
$(NH_4)_6P_2Mo_{18}O_{62}$ [16,17]	975 [17]–979 [16]	715	653	385		
$H_6P_2Mo_{18}O_{62}$ [16]	996	823	668			
$(NH_4)_3PMo_{12}O_{40}$ [19]	984	968	919–877	603		
$H_3PMo_{12}O_{40}$ [20–22]	995.5 [22]; 998 [20,21]	980 [22]	972 [22]; 975 [20,21]	905.5 [22]; 909 [20]; 909–876 [21]	870 [22]	603	251
MoO_3 [7]	998	822	668	285		

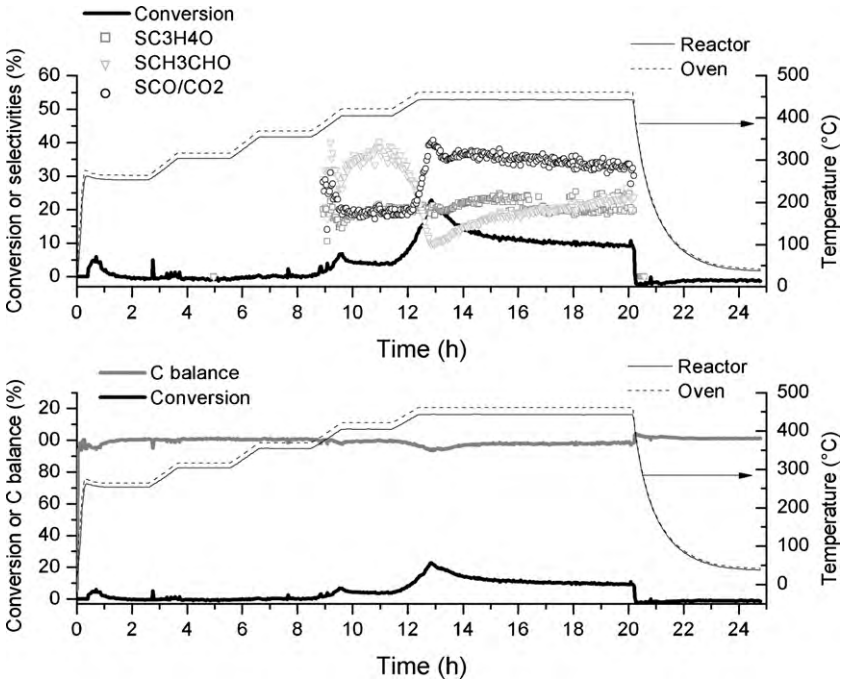

Fig. 6. Catalytic performances obtained for the $(NH_4)_6P_2Mo_{18}O_{62}$ sample under a gaseous mixture of 70 vol.% He, 10 vol.% C_3H_6 and 20 vol.% O_2 ($O_2/C_3H_6 = 2$): (A) conversion of propene and selectivities in acrolein (SC_3H_4O), acetaldehyde (SCH_3CHO), CO and CO_2 (SCO/CO_2) and (B) carbon balance. Below 350 °C, as the catalyst exhibits a weak conversion, determination of selectivities is too delicate.

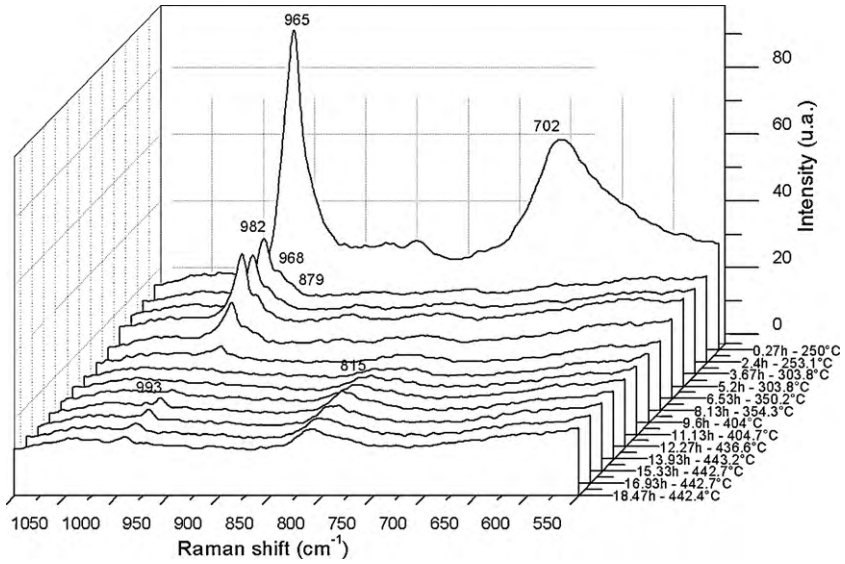

Fig. 7. Raman spectra measured during the catalytic test of the $(NH_4)_6P_2Mo_{18}O_{62}$ sample under a gaseous mixture of 70 vol.% He, 10 vol.% C_3H_6 and 20 vol.% O_2 ($O_2/C_3H_6 = 2$), data below 550 cm^{-1} were not shown.

signal at 982 cm^{-1} (with a shoulder at 968 cm^{-1}) and a small peak at 879 cm^{-1}. This reveals that during this plateau, the sample progressively acquires a Keggin structure [19]. The same Raman signals are observed during the plateau at 300 °C. At 400 °C, a Raman signal at 815 cm^{-1} appears, this is characteristic of the formation of MoO_3[17]. The intensity of this signal increases with time on stream, and at 450 °C, another Raman signal which could be related to MoO_3 appears at 993 cm^{-1}[7].

In order to check if the increase of the conversion observed during the test under a O_2/C_3H_6 ratio of 2 is mainly dictated by the presence of a MoO_3 phases formed *in situ*, the catalytic behavior of $H_3PMo_{12}O_{40}$, $(NH_4)_3PMo_{12}O_{40}$ and Mo trioxide samples along the same temperature profile and under the same gas conditons were compared with that of the Wells–Dawson sample. The results obtained for the tests with Keggin samples are summarized in Figs. 8 and 10, respectively. Concerning the catalytic behavior of a $H_3PMo_{12}O_{40}$ sample, it can be observed that during the first part of the test, the propene conversion follows the temperature. Then, during the temperature rise from 300 to 350 °C, the conversion increases up to 20% followed by a decrease and a stabilization at 15%. A higher increase of conversion (up to 40%) is observed between 350 and 400 °C. This increase is followed by a decrease during the temperature plateau. Finally, between 400 and 450 °C, a slight increase of conversion is observed followed by a stabilisation. During this test, the selectivity toward CO/CO_2 follows the same tendency as the conversion. Moreover, selectivities towards

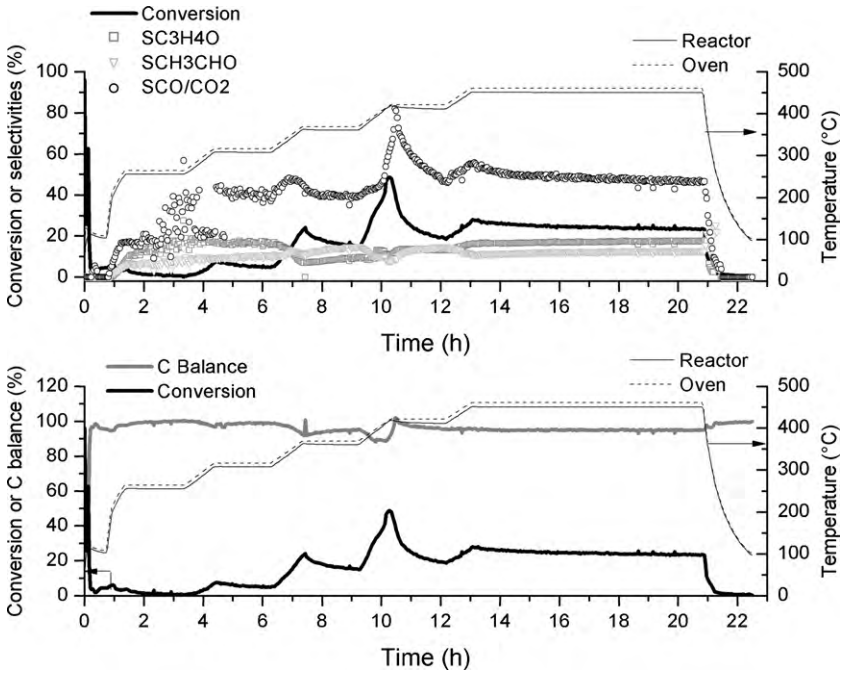

Fig. 8. Catalytic performances obtained for the $H_3PMo_{12}O_{40}$ sample under a gaseous mixture of 70 vol.% He, 10 vol.% C_3H_6 and 20 vol.% O_2 ($O_2/C_3H_6 = 2$): (A) conversion of propene and selectivities in acrolein (SC_3H_4O), acetaldehyde (SCH_3CHO), CO and CO_2 (SCO/CO_2) and (B) carbon balance.

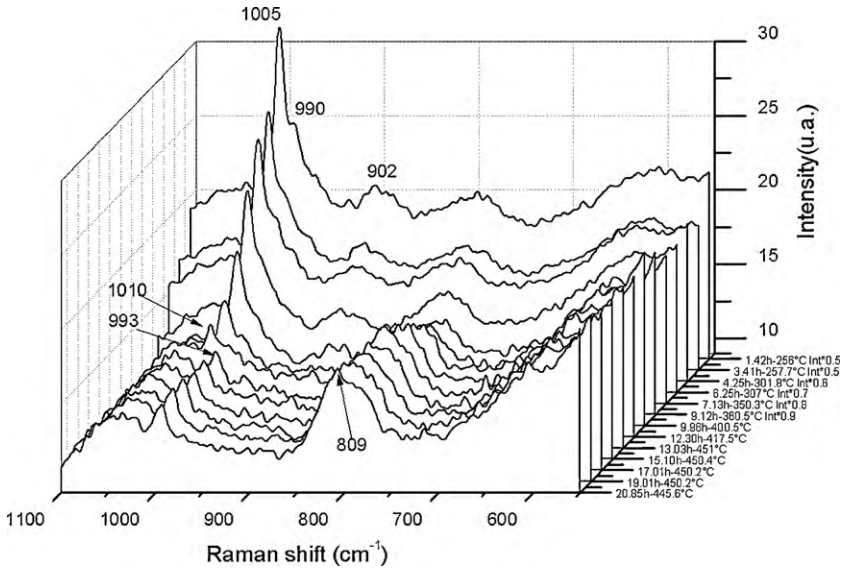

Fig. 9. Raman spectra measured during the catalytic test of the $H_3PMo_{12}O_{40}$ sample under a gaseous mixture of 70 vol.% He, 10 vol.% C_3H_6 and 20 vol.% O_2 ($O_2/C_3H_6 = 2$), data below 550 cm^{-1} were not shown.

acrolein and acetaldehyde products remain at a relatively stable level. It can be noticed that during this test, a slight exothermicity is observed at 400 °C. This phenomena is clearly observed to a higher extend during the catalytic test with $(NH_4)_3PMo_{12}O_{40}$ sample (Fig. 10). Moreover, the reactivity of $(NH_4)_3PMo_{12}O_{40}$ sample seems to be higher than $H_3PMo_{12}O_{40}$ sample. Indeed, the highest level of conversion is 55% at 250 °C. The high reactivity can be related to thermal rearrangement of the $(NH_4)_3PMo_{12}O_{40}$ sample probably due to the loss of nitrogen and water in the temperature window 180–240 °C. This was reported in [8] where $(NH_4)_3PMo_{12}O_{40}$ sample was analysed by thermogravimetric analysis and temperature-programmed decomposition in the temperature range 25–450 ° C in a stream of air. Regarding the Raman spectra (Figs. 9 and 11), molecular modification of the structure of the catalyst and the subsequent formation of a MoO_3 phase begin at approximately 350 °C. Catalytic results and the Raman spectra measured during the test with a Mo trioxide sample are presented in Figs. 12 and 13., respectively. No modifications of the Raman features are noticed during the test; the main Raman bands typical of MoO_3 (995, 817, 666 and 288 cm^{-1}) are observed during the whole experiment. Regarding the catalytic results it can be noticed that the conversion seems to follow the temperature. The conversion curve shows three increases, each one is followed by a stabilization. Firstly, an increase of conversion is observed up to 5%; secondly, the conversion increases up to 20% and finally, a third increase of conversion up to 30% is observed. As already observed, the same behavior is obtained for the selectivity towards CO/CO_2 products (SCO/CO_2). The selectivity for acrolein (SC_3H_4O)

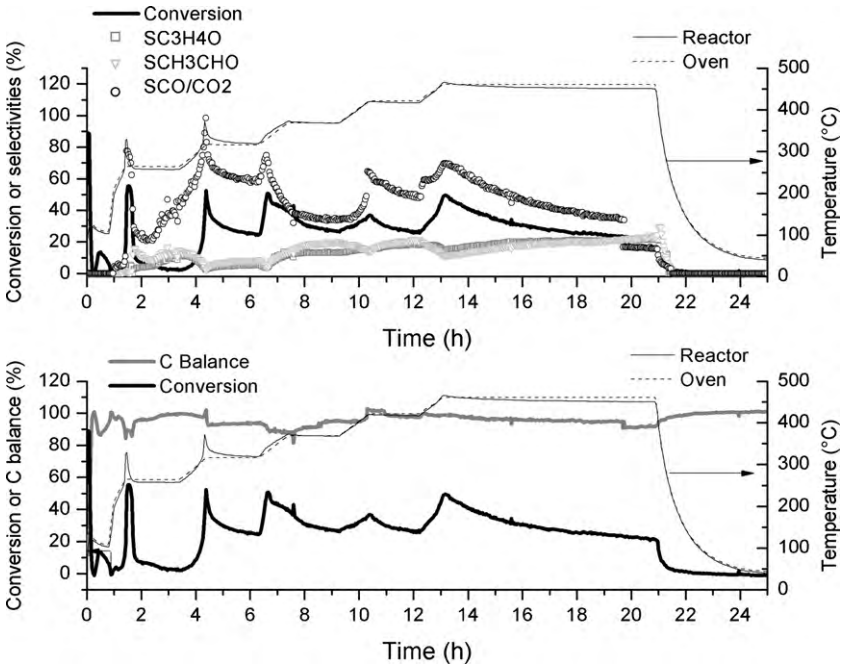

Fig. 10. Catalytic performances obtained for the $(NH_4)_3PMo_{12}O_{40}$ sample under a gaseous mixture of 70 vol.% He, 10 vol.% C_3H_6 and 20 vol.% O_2 ($O_2/C_3H_6 = 2$); (A) conversion of propene and selectivities in acrolein (SC_3H_4O), acetaldehyde (SCH_3CHO), CO and CO_2 (SCO/CO_2) and (B) carbon balance.

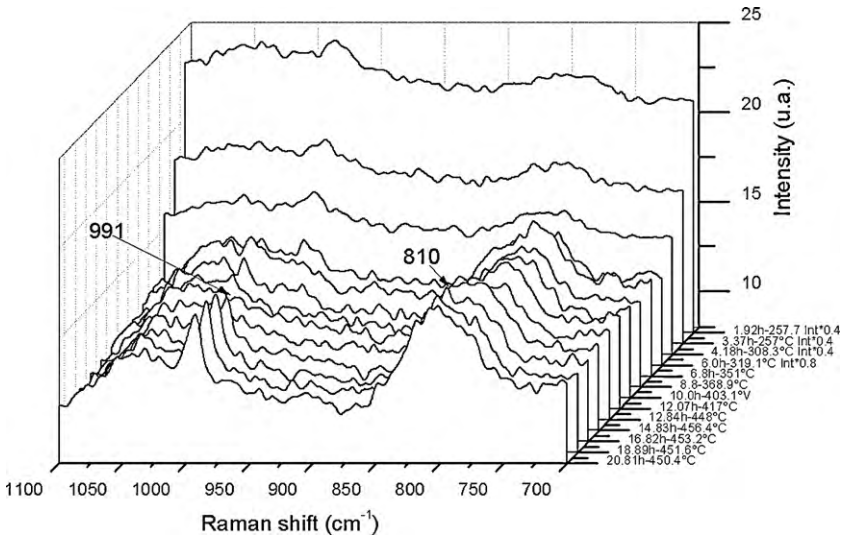

Fig. 11. Raman spectra measured during the catalytic test of the $(NH_4)_3PMo_{12}O_{40}$ sample under a gaseous mixture of 70 vol.% He, 10 vol.% C_3H_6 and 20 vol.% O_2 ($O_2/C_3H_6 = 2$), data below 700 cm^{-1} were not shown.

remains at a stable level (10%) during the whole experiment and the selectivity for acetaldehyde (SCH_3CHO) reveals a decrease from 25 down to 10% before the plateau at 400 °C.

Catalytic results obtained with the O_2/C_3H_6 ratios of 0.5 and 1 in the reaction feed are plotted in Figs. 16 and 14. Raman spectra, recorded during these tests, are presented in Figs. 17 and 15, respectively for O_2/C_3H_6 ratios of 0.5 and 1. Similar results were observed for the two atmospheres. Concerning the catalytic tests, a peak of propene conversion (15 and 20% for O_2/C_3H_6 ratios of 0.5 and 1 respectively) is observed at the beginning of the plateau at 450 ° C followed by a stabilization at 10%. During this peak of conversion, all the selectivities reveal a decreasing trend followed by an increasing trend and a stabilization. Besides, the carbon balance curves (Figs. 16(B) and 14(B)) exhibit a marked decrease at the same time as the conversion increases. These, and the fact that at this moment less products are formed at the outlet, allow to hypothesize that propene seems to be trapped by the catalyst. This phenomenon is reversible as at the end of the temperature plateau and the beginning of the cooling step under the reaction gaz, it can be noticed that the carbon balance curve increases up to 130%. The observation that this excess carbon was recovered as propene (and not as CO/CO_2) allows unambigously to discard the possibility that the 'missing' propene at 450 ° C was stored as coke at the surface of the sample. Regarding Raman spectra recorded during the test with the O_2/C_3H_6 ratios of 0.5 (Fig. 17), it can be observed that the Raman spectrum measured at the beginning of the plateau at 250 °C, reveals signals at 966 and 711 cm^{-1} (with a shoulder at 645 cm^{-1}), while the Raman spectrum measured at the end of this

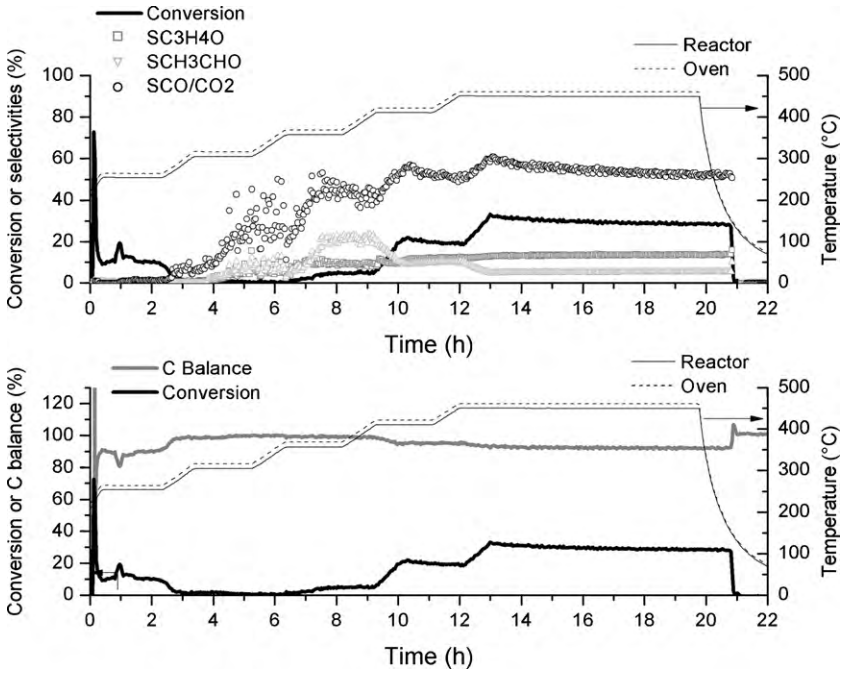

Fig. 12. Catalytic performances obtained for the MoO_3 sample under a gaseous mixture of 70 vol.% He, 10 vol.% C_3H_6 and 20 vol.% O_2 ($O_2/C_3H_6 = 2$): (A) conversion of propene and selectivities in acrolein (SC_3H_4O), acetaldehyde (SCH_3CHO), CO and CO_2 (SCO/CO_2) and (B) carbon balance.

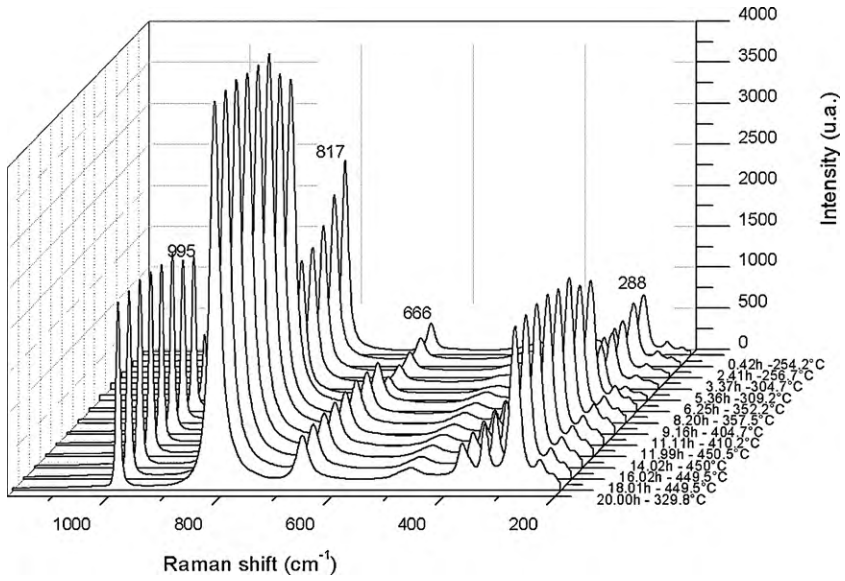

Fig. 13. Raman spectra measured during the catalytic test of the MoO_3 sample under a gaseous mixture of 70 vol.% He, 10 vol.% C_3H_6 and 20 vol.% O_2 ($O_2/C_3H_6 = 2$)

plateau, presents a signal at 981 (with a shoulder at 966). In addition, the signal at 711 cm^{-1} disappears during this step. As observed during the catalytic test under a O_2/C_3H_6 ratio of 2, the molecular structure of the catalyst is modified during the stabilization at 250 °C, and the sample acquires a Keggin structure during this step [19]. The Raman spectra recorded at 300 °C, confirmed this modification as a peak at 871 cm^{-1}, typical of a Keggin molecular structure, appears [19]. No further interpretation of the spectrum after 400 ° C can be done due to some defocusing of the laser beam on the solid probably because the conditions for recording change during the heating and because of the reduce of the volume of the catalyt bed observed during tests under reductive feeds. The defocusing of the laser beam on the catalyst is unfortunately also observed during the catalytic test with O_2/C_3H_6 ratio of 1 in a more marked manner than with the O_2/C_3H_6 ratio of 0.5. As a result, no proper interpretation of the molecular evolution of the catalyst can be done in this case.

4. Discussion

This study shows that features of the Wells–Dawson heteropolycompound catalyst can to be tuned by the oxido-reduction properties of the gaseous atmosphere during a thermal treatment. Typically, the thermal treatment induces modifications inside the structure of the Wells–Dawson which occur through two steps. A first step leads to the formation of the Keggin compound and a second step where the *in situ* formed Keggin compound is further decomposed to yield oxide species. Looking at the influence of the

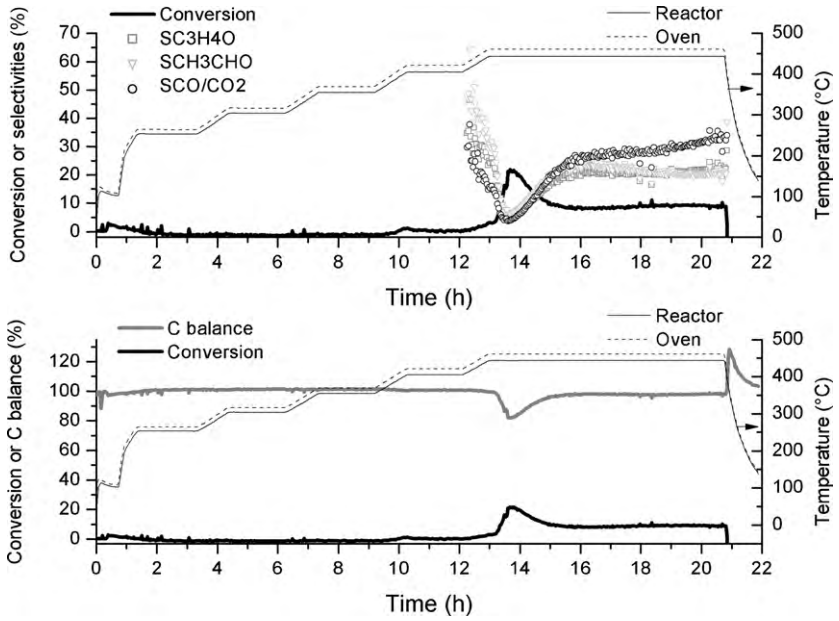

Fig. 14. Catalytic performances obtained for the $(NH_4)_6P_2Mo_{18}O_{62}$ sample under a gaseous mixture of 80 vol.% He, 10 vol.% C_3H_6 and 10 vol.% O_2 ($O_2/C_3H_6 = 1$): (A) conversion of propene and selectivities in acrolein (SC_3H_4O), acetaldehyde (SCH_3CHO), CO and CO_2 (SCO/CO_2) and (B) carbon balance. Below 350 °C, as the catalyst exhibits a weak conversion, determination of selectivities is too delicate.

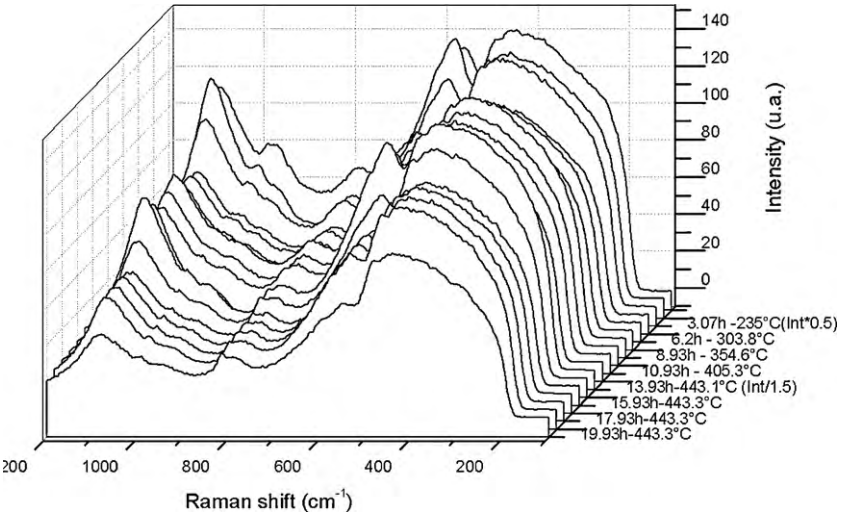

Fig. 15. Raman spectra measured during the catalytic test of the $(NH_4)_6P_2Mo_{18}O_{62}$ sample under a gaseous mixture of 80 vol.% He, 10 vol.% C_3H_6 and 10 vol.% O_2 ($O_2/C_3H_6 = 1$).

composition of the gas phase, we observed some adjustments inside this rearrangement process both by *in situ* XRD and *in situ* Raman investigations. The presence of oxygen appears to play a key role in this process. The hypothesis on the role of oxygen is that it would restore the catalyst to its initial state while a 'less oxidizing' atmosphere would limit such effect. This stabilizing effect of oxygen could appear surprising in the frame of a decomposition of a structure to fully oxidic species. At this stage, one should thus mention that the number of oxygen atoms per molybdenum is higher in Wells–Dawson (namely 3.44) than in Keggin (namely 3.33) and in MoO_3 (namely 3). The hypothesis would be that this parameter, more than the number of oxygen atoms per indistinct metal, is dictating the system. Thus, a reductive feed would promote the reorganisation of the Wells–Dawson heteropolyanion into a structure where the needed number of oxygen atoms per molybdenum is smaller, as it is the case for Keggin structure, compared to the initial state. On the contrary, an oxidizing feed would slow down the rearrangement process. As a result, the Wells–Dawson crystalline and molecular structure remains intact up to a higher temperature under an oxidizing atmophere compared to both inert and reducing feeds. This hypothesis is also supported by the subsequent rearrangement of the Keggin anion into oxide species. Indeed, the crystalline structures of oxide species appear at a higher temperature under the oxidizing feed. Thus, the role of oxygen is confirmed. Unlike the influence of an oxidizing atmosphere, a reductive atmosphere promotes the rearrangement of the Keggin into new structures where the number of oxygen atoms per molybdenum is smaller, as it is the case in MoO_3. These observations are also in agreement with our preliminary studies [8,9]. Indeed, we observed that under a reducing feed, the rearrangement of the Wells–Dawson sample and the subsequent presence of the particular species, with most desired enhanced performances in selective oxidation processes, would start immediately, in contrast to what happens under a

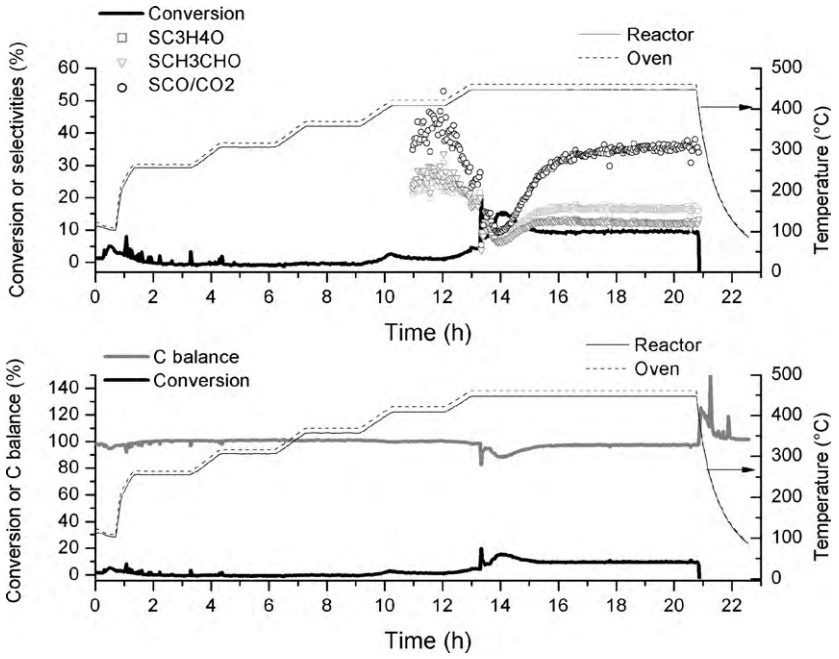

Fig. 16. Catalytic performances obtained for the $(NH_4)_6P_2Mo_{18}O_{62}$ sample under a gaseous mixture of 75 vol.% He, 10 vol.% C_3H_6 and 5 vol.% O_2 ($O_2/C_3H_6 = 0.5$): (A) conversion of propene and selectivities in acrolein (SC_3H_4O), acetaldehyde (SCH_3CHO), CO and CO_2 (SCO/CO_2) and (B) carbon balance. Below 350 °C, as the catalyst exhibits a weak conversion, determination of selectivities is too delicate.

more oxidizing feed. The oxydo-reduction properties of the gaseous atmosphere is indeed a tool to control the reorganisation of Wells–Dawson salt and it may be used to modulate the catalytic performances of heteropolycompound catalysts.

Regarding the catalytic test under a O_2/C_3H_6 ratio of 2, the main observation is that there is an increase of propene conversion (Fig. 6) related to the *in situ* formation of a molybdenum oxide phase (Raman results Fig. 7). This observation is supported by the catalytic tests with Keggin heteropolycompounds. Nevertheless, the conversion of propene is never boosted with the MoO_3 catalyst (Fig. 13). So, the observed increase of conversion could not be explained by the *in situ* formation of a well-defined Mo trioxide. Our previous studies evoked that the highest performances were obtained on a 'living' catalyst, likely with a wobbly structure, that was formed *in situ* [8,9]. Indeed, it was found that a particular species, formed *in situ* and presenting intermediate charcteristics between those of Wells–Dawson and Keggin structure, exerts a beneficial effect on the selectivity to the oxidative dehydrogenation path [8,9]. It now seem that in the present case, the conversion of propene is boosted while the working catalyst is in the course of its rearrangement between a keggin structure and that of molybdenum oxide phase. Investigating the effect that our newly acquired tool, namely playing with the oxido-reductive strength of the atmosphere, could bring on the catalytic activity (results obtained under O_2/C_3H_6 ratios of 1 and 0.5; Figs. 14 and 16, respectively) can help to understand the nature of this active species.

Under O_2/C_3H_6 ratios of 1 and 0.5, an increase of the conversion is also observed. But, this increase is not linked to any increase of

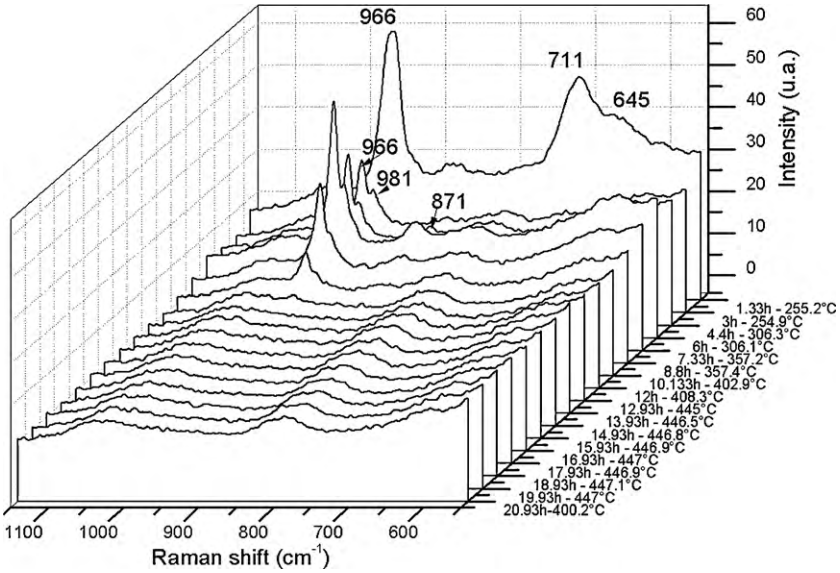

Fig. 17. Raman spectra measured during the catalytic test of the $(NH_4)_6P_2Mo_{18}O_{62}$ sample under a gaseous mixture of 75 vol.% He, 10 vol.% C_3H_6 and 5 vol.% O_2 ($O_2/C_3H_6 = 0.5$). The Raman spectra were rescaled in order to more clearly evidence the modifications.

the selectivity to acrolein which allowed to hypothesize that propene was trapped by the catalyst in a reversible way (Figs. 14 and 16). Moreover, during these experiments, we have noticed a reduction of the catalytic volume bed at the end of the test compared to what was observed under a O_2/C_3H_6 ratio of 2. These two facts evidence that a reductive gaseous feed brings a particular behavior of Wells–Dawson heteropolycompound samples. Looking in more details the C balance concerning the catalytic test under a O_2/C_3H_6 ratio of 2 (Fig. 6), it can be observed that the carbon balance also shows a small decrease at the moment when that the conversion increases. So, whatever the gaseous conditions, the working catalyst trapped the propene but this phenomenon seems to be facilitated by a more reductive atmosphere. The increase of acrolein production observed during the test under a O_2/C_3H_6 ratio of 2 may thus be explained by the formation of a special molybdenum trioxide looking phase (in the sense that it is structurally close to MoO_3 as observed by Raman, but that it is not MoO_3 as the catalytic behavior of pure MoO_3 does not fit) which can trap propene and the formation of this special phase seems to be facilitated by a reductive atmosphere.

A possible explanation comes from our investigation of the litterature concerning molybdenum oxide based catalysts. Molybdenum oxide based systems are highly active heterogeneous catalysts for the selective oxidation of hydrocarbons [23]. Nevertheless the catalytically active phases appear to be neither MoO_3 nor MoO_2 but rather a partially reduced molybdenum oxide, numerous studies were done on phase evolution and kinetics of the reduction of MoO_3 to MoO_2[24–26]. It is well-known that Mo trioxide can release oxygen atoms in reductive conditions, to form 'substoichiometric' oxides as $Mo_{18}O_{52}$ and Mo_8O_{23}[27]. These can rapidly reincorporate missing oxygen, to reform MoO_3 but they can also rapidly give additional oxygen, making that they can undergo the Mars and Van Krevelen mechanism more easily, thus bringing more activity. During allylic oxidation, the surface of MoO_3 cyclically reduces and reoxidizes, this corresponding to the alternate formation of selective 'corner-sharing' (oxidized) and less selective 'edge-sharing' (reduced) MoO_6^{6-} octahedra [27]. Ressler et al. [26] investigated the early stage of the reduction of MoO_3 with hydrogen; in particular, structural changes in MoO_3 or the evolution of phases prior to the formation of MoO_2 by performing *in situ* X-ray diffraction and *in situ* X-ray absorption spectroscopy on the temperature-programmed reduction of MoO_3 in hydrogen. The first step of the simplified mechanism proposed is the incorporation of H_2 in the MoO_3 bulk and formation of a more or less ordered bronze(H_xMoO_{3-x}). The H_xMoO_{3-x} is formed in the early stage of the reduction to MoO_2 and is consumed prior to the complete reduction of MoO_3 to MoO_2. Formation of bronze was also reported in litterature concerning heteropolycompound catalysts. According to Mioc et al. [28], Keggin anions are transformed at about 600 °C in a new monophosphate bronze type compound. Indeed, Mioc et al. [28] investigated the phase transformation of 12-tungstophosphoric acid 29-hydrate, namely $H_3PW_{12}O_{40}$-$29H_2O$, in the temperature range from ambient temperature to 1150 °C. Dehydration process modified the protonic species equilibrium and a phosphorus-containing bronze, PW_8O_{26} is reported to be synthesize from Keggin's anion framework as a precursor by solid-solid recrystallization [28]. The bronze is viewed as a three-dimensional network of WO_6 octahedra filled with PO_4 tetrahedra [28]. Despite no litterature concerning the formation of bronze from molybdenum-based heteropolycompound precursors was found, a plausible hypothesis is that heteropolycompound catalysts rearrange into a bronze like structure with a three-dimensional network of molybdenum oxide whith channels filled with propene. This is a believable possibility as similar configurations have already been observed, respectively, for Te in $TeMo_5O_{16}$[29] and for Sb in $Sb_2Mo_{10}O_{31}$[30,31]. Indeed, as reported by [32], Tellerium (or antimony) cations and oxygen anions can occupy channels in MoO_6 lattice. With respect to this litterature, it's possible that propene molecules fill the formed channels in the bronze like structure. The catalytic results reveal that the formation of such propene-containing bronze looking structure seems to be facilitated under a reductive atmosphere. Indeed, under a reductive feed, Mo based catalysts release oxygen atoms and thus would be more able to change their configuration. With this new configuration, the catalyst could more easily alternate the formation of 'corner-sharing' and 'edge-sharing' MoO_6^{6-} octahedra and this may explained why the catalytic activity is improved. This speculative hypothesis concerning the formation of a bronze looking structure should be verified by further investigations.

5. Conclusions

The reorganisation of $(NH_4)_6P_2Mo_{18}O_{62}$ heteropolycompound sample into oxide species is depending on the oxido-reduction strength of the gaseous feed. This paper shows that gaseous oxygen plays a key role during the rearrangement process. Indeed, this process is promoted by a 'less oxidizing atmosphere' and slowed down by an oxidizing atmosphere. In other words, an oxidizing feed stabilizes the heteropolycompound sample. As a consequence, the oxido-reduction properties of the gaseous feed can be used to modulate the catalytic activities of heteropolycompound catalysts.

The catalytic behavior of $(NH_4)_6P_2Mo_{18}O_{62}$ in the oxidation of propene varies at increasing temperature. In particular, a peak of propene conversion is observed under a gaseous O_2/C_3H_6 ratio of 2. Looking for the influence of the oxido-reduction atmosphere, it was shown that, under gaseous O_2/C_3H_6 ratio of 1 and 0.5, propene was trapped in the catalyst in a reversible way. This phenomenon was observed under a ratio of 2 although to a less marked manner. As a consequence, the observed increase of propene conversion might be due to the presence of a propene-containing bronze looking structure. This speculative configuration may allow the catalyst to easily alternate the formation of corner-sharing and edge-sharing MoO_6^{6-} octahedra and this may explain that the conversion of propene is boosted.

Acknowledgments

The authors thank the Université catholique de Louvain for the financial support and the teaching assistant - PhD student position of E.A. The authors wish also to thank the 'Fonds National de la Recherche Scientifique' (Belgium) for the acquisition of the XPS equipment. This research is part of a Concerted Research Action of the "Communauté Française de Belgique" allotted by the Académie Universitaire Louvain. The involvement of Unité de catalyse et de chimie des matériaux divisés in the 'Inanomat' IUAP network sustained by the 'Service public fédéral de programmation politique scientifique' (Belgium) is also acknowledged. The Unité de catalyse et chimie des matériaux divisés is also involved in the 'EMMI' European Multifunctionnal Material Institute built from the previous 'FAME' Network of Excellence of the EU 6th FP, and in the Cost Action D41 sustained by the European Science Foundation.

References

[1] M. Pope, Heteropoly and Isopoly Oxometalates, Springe-Verlag, New York, 1983.
[2] M. Misono, Catal. Rev. Sci. Eng. 29 (1987) 269–321.
[3] I. Kozhevnikov, Catal. Rev. Sci. Eng. 37 (1995) 311–352.
[4] I. Kozhevnikov, Chem. Rev. 98 (1998) 171–198.
[5] T. Okuhara, N. Mizuno, M. Misono, Adv. Catal. 41 (1996) 113–252.
[6] F. Cavani, Catal. Today 41 (1998) 73–86.
[7] G. Mestl, T. Ilkenhans, D. Spielbauer, M. Dieterle, O. Timpe, J. Krohnert, F. Jentoft, H. Knozinger, R. Schlogl, Appl. Catal. A: Gen. 210 (2001) 13–34.

[8] E. Arendt, K.M. McEvoy, E.M. Gaigneaux, Appl. Catal. A: Gen. 357 (2009) 115–124.
[9] E. Arendt, E. Charlier, E.M. Gaigneaux, Top. Catal 52 (2009) 1232–1241.
[10] H. Wu, J. Biol. Chem. 43 (1920) 189–220.
[11] M. Sultan, J. Livage, J. Launay, M. Fournier, Y. Jeannin, J. Am. Chem. Soc. 104 (1982) 3194–3202.
[12] E. Gaigneaux, H.A. Dayem, E. Godard, P. Ruiz, Appl. Catal. A: Gen. 202 (2000) 265–283.
[13] J.F. Moulder, W. Stickel, P. Sobol, K. Bomben, Handbook of X-ray Photoelectron Spectroscopy, in: J. Chastain (Ed.), PerkinElmer Corporation, Eden Prairie, MN, 1992.
[14] T. Nijhuis, S. Tinnemans, T. Visser, B. Weckhuysen, Phys. Chem. Chem. Phys. 5 (2003) 4362–4365.
[15] T. Nijhuis, S. Tinnemans, T. Visser, B. Weckhuysen, Chem. Eng. Sci. 59 (2004) 5487–5492.
[16] L. Briand, G. Valle, H. Thomas, J. Mater. Chem. 12 (2002) 299–304.
[17] G. Valle, S. Matkovic, L. Gambaro, L. Briand, Catalyst Preparation—Science and Engineering, chap. The Environmentally Friendly Synthesis of Heteropolyacids, CRC Press, 2007, pp. 75–92.
[18] F. Dury, E.M. Gaigneaux, Catal. Today 117 (2006) 46–52.
[19] C. Srilakshmi, N. Lingaiah, I. Suryanarayana, P. Prasad, K. Ramesh, B. Anderson, J. Niemantsverdriet, Appl. Catal. A: Gen. 296 (2005) 54–62.
[20] C. Rocchiccioli-Deltcheff, A. Aouiss, S. Launay, M. Fournier, J. Mol. Catal. A: Chem. 114 (1996) 331–342.
[21] C. Rocchiccioli-Deltcheff, A. Aouissi, M.M. Bettahar, S. Launay, M. Fournier, J. Catal. 164 (1996) 16–27.
[22] C. Rocchiccioli-Deltcheff, M. Fournier, R. Franck, R. Thouvenot, Inorg. Chem. 22 (1983) 207–216.
[23] J. Haber, E. Lalik, Catal. Today 33 (1997) 119–137.
[24] J.R. Regalbuto, J.-W. Ha, Catal. Lett. 29 (1994) 189.
[25] T. Ressler, R. Jentoft, J. Wienold, M. Gunter, O. Timpe, J. Phys. Chem. B 104 (2000) 6360.
[26] T. Ressler, J. Wienold, R.E. Jentoft, Solid State Ionics 141–142 (2001) 243–251.
[27] E. Gaigneaux, P. Ruiz, E. Wolf, B. Delmon, Appl. Surf. Sci. 121/122 (1997) 552–557.
[28] U. Mioc, M. Todorovic, M. Davidovic, P. Colomban, I. Holclajtner-Antunovic, Solid State Ionics 176 (2005) 3005–3017.
[29] P. Forestier, M. Goreaud, C. R. Acad. Sci. Paris 312 (Serie II) (1991) 1141.
[30] M. Parmentier, C. Gleitzer, A. Courtois, J. Protas, Acta Crystallogr. B 35 (1963) 1979.
[31] E.M. Gaigneaux, M. Dierterle, P. Ruiz, G. Mestl, B. Delmon, J. Phys. Chem. B 102 (1998) 10542–10555.
[32] J. Millet, M. Baca, A. Pigamo, D. Vitry, W. Ueda, J. Dubois, Appl. Catal. A: Gen. 244 (2003) 359–370.